

Dynamic polarizabilities of the clock states of Al^+

Yuan-Fei Wei(魏远飞), Zhi-Ming Tang(唐志明), Cheng-Bin Li(李承斌), Yang Yang(杨洋), Ya-Ming Zou(邹亚明), Kai-Feng Cui(崔凯枫), and Xue-Ren Huang(黄学人)

Citation: Chin. Phys. B, 2022, 31 (**8**): 083102. DOI: 10.1088/1674-1056/ac5880
Journal homepage: http://cpb.iphy.ac.cn; http://iopscience.iop.org/cpb

What follows is a list of articles you may be interested in

Calculations of dynamic multipolar polarizabilities of the Cd clock transition levels

Mi Zhou(周密) and Li-Yan Tang(唐丽艳)
Chin. Phys. B, 2021, 30 (**8**): 083102. DOI: 10.1088/1674-1056/abf0fc

Charge disturbance/excitation in the Raman virtual state revealed by ROA signal: A case study of pinane

Ziqi Zhu(祝子祺), Peijie Wang(王培杰), and Guozhen Wu(吴国祯)
Chin. Phys. B, 2021, 30 (**6**): 063101. DOI: 10.1088/1674-1056/abea90

Calculations of atomic polarizability for beryllium using MCDHF method

Hui Dong(董辉), Jun Jiang(蒋军), Zhongwen Wu(武中文), Chenzhong Dong(董晨钟), and Gediminas Gaigalas
Chin. Phys. B, 2021, 30 (**4**): 043103. DOI: 10.1088/1674-1056/abd92d

Finite-field calculation of electric quadrupole moments of $^2P_{3/2}$, $^2D_{3/2,5/2}$, and $^2F_{5/2,7/2}$ states for Yb^+ ion

Xi-Tong Guo(郭希同), Yan-Mei Yu(于艳梅), Yong Liu(刘永), Bing-Bing Suo(索兵兵)
Chin. Phys. B, 2020, 29 (**5**): 053101. DOI: 10.1088/1674-1056/ab821c

Analytical expressions of non-relativistic static multipole polarizabilities for hydrogen-like ions

Xuesong Mei(梅雪松), Wanping Zhou(周挽平), Zhenxiang Zhong(钟振祥), Haoxue Qiao(乔豪学)
Chin. Phys. B, 2020, 29 (**4**): 043101. DOI: 10.1088/1674-1056/ab75d0

Dynamic polarizabilities of the clock states of Al^+

Yuan-Fei Wei(魏远飞)[1,3,4,†], Zhi-Ming Tang(唐志明)[2,†], Cheng-Bin Li(李承斌)[1,‡], Yang Yang(杨洋)[2,§], Ya-Ming Zou(邹亚明)[2], Kai-Feng Cui(崔凯枫)[1,4], and Xue-Ren Huang(黄学人)[1,4,¶]

[1] *State Key Laboratory of Magnetic Resonance and Atomic and Molecular Physics, Innovation Academy for Precision Measurement Science and Technology, Chinese Academy of Sciences, Wuhan* 430071, *China*
[2] *Shanghai EBIT Laboratory, Key Laboratory of Nuclear Physics and Ion-Beam Application (MOE), Institute of Modern Physics, Fudan University, Shanghai* 200433, *China*
[3] *University of Chinese Academy of Sciences, Beijing* 100049, *China*
[4] *Key Laboratory of Atom Frequency Standards, Innovation Academy for Precision Measurement Science and Technology, Chinese Academy of Sciences, Wuhan* 430071, *China*

(Received 4 December 2021; revised manuscript received 4 February 2022; accepted manuscript online 25 February 2022)

The dynamic polarizabilities of $3s^2\,{}^1S_0$ and $3s3p\,{}^3P_0^o$ states of Al^+ are calculated using the hybrid configuration interaction and many-body perturbation theory method, and multiconfiguration Dirac–Hartree–Fock method in this work. Five ultraviolet magic wavelengths for the Al^+ clock transition $3s^2\,{}^1S_0$–$3s3p\,{}^3P_0^o$ are predicted. Although the suitable lasers are not available presently, the potential precision measurement on these magic wavelengths for the Al^+ clock transition would be used to extract the ratios of several certain transition matrix elements with high accuracy, and then help to improve the precision and reliability of the estimate of the BBR shift of the Al^+ clock transition. The differential dynamic polarizabilities at certain wavelengths are evaluated, which are useful to assess the ac Stark shift of the Al^+ clock transition frequency and helpful in the clock experiments to suppress the ac Stark shift of the clock transition as possible as it can.

Keywords: dynamic polarizability, Al^+ optical clock

PACS: 31.15.ap, 31.15.am, 32.60.+i **DOI:** 10.1088/1674-1056/ac5880

1. Introduction

Optical frequency standards have important application prospects in local timekeeping, deep space satellite navigation and the test of the fundamental theory of physics.[1–4] In recent years, the optical frequency standards based on neutral atoms or trapped ions have made great development[5–9] and some of them have demonstrated fractional frequency uncertainties of a few parts in 10^{-18} or even 10^{-19}. Among them, the Al^+ optical clock based on the trapped Al^+ ion has been well developed in the past decades due to the application of the sympathetic cooling and quantum-logic technologies.[10] In 2010, NIST researchers realized the comparison of two aluminum ion optical clocks and the frequency uncertainty reached 8.6×10^{-18}.[11] They improved their experimental setups in 2019 and achieved the systematic uncertainty of 9.4×10^{-19}.[9]

The Al^+ optical clock is working on the highly forbidden $3s^2\,{}^1S_0$–$3s3p\,{}^3P_0^o$ transition and the black-body radiation (BBR) shift of this transition is predicted to be very small.[12] Not only the intrinsic characters of Al^+, which are insensitive to environmental perturbations, but also the delicate technologies of sympathetic cooling and quantum logic spectroscopy, make the Al^+ optical clock capable of achieving extreme precisions. To provide the reliable systematic uncertainty budget for the Al^+ optical clock, all the perturbations to the clock transition should be carefully considered, including the motional effects of the working ions, BBR shift of the clock transitions, frequency shifts due to the external electromagnetic fields, and so on. The BBR shift is generally associated with the differential static polarizabilities of the clock working states.[13] In the Al^+ clock, Mg^+ or Ca^+ is usually adopted for the sympathetic cooling of Al^+.[9,11,14] The Doppler cooling laser beam of Mg^+ or Ca^+ maintains the Al^+–Mg^+ or Al^+–Ca^+ pair at a constant motional temperature during the clock interrogation pulse. Because it is also shed on the Al^+ ions, it causes an ac Stark shift to the clock transition, which is associated with the differential dynamic polarizabilities of the clock working states.

The polarizability of an atomic system describes the distortion in the charge distribution and gives a measure of the energy shift of the atomic system when it is exposed in an electromagnetic field.[12,15] Since precise measurement of polarizabilities is quite challenging, the reliable and accurate theoretical studies of atomic and ionic polarizabilities are of particular interest. In the case of Al^+, the previous studies are mainly focused on the static polarizabilities[16–19] to evaluate the BBR contribution to the fractional frequency uncertainty of the clock transtion. Rosenband *et al.* used an extrapolation expression to estimate the dynamic polarizabili-

[†]These authors contributed equally to this work.
[‡]Corresponding author. E-mail: cbli@apm.ac.cn
[§]Corresponding author. E-mail: yangyang@fudan.edu.cn
[¶]Corresponding author. E-mail: hxueren@apm.ac.cn

© 2022 Chinese Physical Society and IOP Publishing Ltd

ties of the $3s^2\,{}^1S_0$ and $3s3p\,{}^3P_0^o$ states of Al^+ at the wavelength $\lambda = 1126$ nm.[20] Although their results agreed with the later theoretical calculations using the configuration interaction plus core polarization (CICP) method[16] and the configuration interaction plus all-order (CI+all-order) method,[18] the wavelength of the electromagnetic radiation adopted in the extrapolation method is required to be far-detuned from all transitions connecting to either clock states. The study on the dynamic polarizabilities over large range of electromagnetic spectrum of Al^+ is still scarce. Such study would not only be useful in the potential experiments based on Al^+, but also lead to the prediction and identification of the magic wavelengths of Al^+ clock transition. The magic wavelength for a transition is the wavelength at which the ac Stark shift of the transition energy is zero,[21] and it means that, for the upper and lower energy levels of the transition concerned, the difference of the dynamic polarizabilities is zero. A notable application of the magic wavelengths is the optical lattice clocks operated on the neutral atoms.[1] As for the atomic ions, the magic wavelengths for the $4s_{1/2}$–$3d_{5/2}$ transition in Ca^+ have been observed, and meanwhile the ratio of the matrix elements for the $4s_{1/2}$–$4p_{1/2}$ and $4s_{1/2}$–$4p_{3/2}$ has been determined.[22] The identification of magic wavelength for ion clock transition pave the milestone for establishing all-optical trapped ion clocks and the precision values of the transition matrix elements extracted from the magic wavelength measurement could be used to improve the precision of the estimation of the BBR shift.

For these motivations, we made calculations of the dynamic polarizabilities of the $3s^2\,{}^1S_0$ and $3s3p\,{}^3P_0^o$ states in Al^+ based on sum-over-states (SOS) approach. The transition matrix elements were obtained using the method combining configuration interaction and the many-body perturbation theory (CI+MBPT),[23] and the multiconfiguration Dirac–Hartree–Fock (MCDHF) method.[24] A brief introduction of the theoretical methods and computational details is given in Section 2. The computation results of the energy levels, transition matrix elements, polarizabilities and magic wavelengths are given and discussed in Section 3.

2. Method of calculations

2.1. Polarizability

The dynamic electric dipole (E1) polarizability of a quantum state v in an electromagnetic radiation generally consists of three contributions from scalar, vector and tensor polarizabilities.[25] Both contributions from vector and tensor polarizabilities are related with the magnetic angular momentum quantum numbers of the atomic state. In this work, $3s^2\,{}^1S_0$ and $3s3p\,{}^3P_0^o$ states in Al^+ will be considered, and total angular momentum quantum numbers J for both states are zero. Thus, only the scalar polarizability will be taken into account, and it can be conveniently divided into three parts:

$$\alpha_v(\omega) = \alpha_{v,\mathrm{v}}(\omega) + \alpha_{v,\mathrm{core}}(\omega) + \alpha_{v,\mathrm{cv}}(\omega), \tag{1}$$

where $\alpha_{v,\mathrm{v}}(\omega)$, $\alpha_{v,\mathrm{core}}(\omega)$, and $\alpha_{v,\mathrm{cv}}(\omega)$ represent the contributions from valence, atomic core and the interaction between core-valence; and $\alpha_{v,\mathrm{v}}(\omega)$ can be expresses as

$$\alpha_{v,\mathrm{v}}(\omega) = \frac{2}{3(2j_v+1)} \sum_{j_\kappa} \frac{|\langle \psi_v \| D \| \psi_\kappa \rangle|^2 \Delta E_{\kappa v}}{\Delta E_{\kappa v}^2 - \omega^2}, \tag{2}$$

where $|\langle \psi_v \| D \| \psi_k \rangle|$ is the reduced matrix element (RME) of E1 transition. $\Delta E_{\kappa v} = E_\kappa - E_v$ is the energy difference between quantum states v and κ. The value of the dynamic polarizability in $\omega \to 0$ limit is the static polarizability.

For an ion in a single-model laser field, the energy shift of a given atomic state v can be written as

$$\Delta E_v = -\alpha_v(\omega) I + O(I^2), \tag{3}$$

where I is the laser intensity, and $O(I^2)$ represents the residual high-order Stark shift which is usually small and can be omitted under the weak intensity limit. The frequency shift of a certain transition caused by the electromagnetic field can be written as

$$h\Delta\nu = \Delta E_\kappa(\omega) - \Delta E_v(\omega) = -\Delta\alpha(\omega) I + \Delta O(I^2), \tag{4}$$

where $\Delta\alpha(\omega)$ is the differential dynamic polarizability of states κ and v. Thus, by ignoring all nonlinear Stark shifts, the magic wavelength can be theoretically given by the condition $\Delta\alpha(\omega) = 0$.[1]

2.2. CI+MBPT calculations

In the present work, CI+MBPT calculations are performed to get the energy levels and RMEs for Al^+ using the program package developed by Kozlov *et al.*[23] The CI+MBPT method is based on a combination of a conventional configuration interaction (CI) method and many-body perturbation theory (MBPT). The former explicitly contains the interaction between valence electrons, while the latter includes core–core and core–valence correlations. The calculations start from the numerical solution of Hartree–Fock–Dirac (HFD) equations using finite difference method to get single-electron HFD energies and wavefunctions for the core and valence electrons. Here, 1s–4s, 2p–4p, 3d–4d and 4f orbitals are taken into account in this step. The virtual orbitals are then constructed by an automatic generation subroutine which is embedded in the package. The maximal principal quantum number $n_{\max}$ and the maximal orbital quantum number $l_{\max}$ are set to be 30 and 4, respectively. The HFD orbitals and the auto-generated virtual orbitals form the basis set (or say, the orbital space) for the later CI and MBPT calculations. The electron configuration of Al^+ can be treated as a close-shell core $[1s^2 2s^2 2p^6]$ and two valence electrons outside the

core. The effective Hamiltonian for two valence electrons in the CI+MBPT method can be written as

$$\hat{H}^{\text{eff}} = \hat{h}_1(r_1) + \hat{h}_1(r_2) + \hat{h}_2(r_1, r_2), \tag{5}$$

where $\hat{h}_1$ and $\hat{h}_2$ are the single-electron and two-electron interaction terms of the relativistic Hamiltonian, respectively. In the standard CI method, $\hat{h}_1$ includes the kinetic energy of the electron, Coulomb interaction with the nucleus and the HFD potential of the close-shell atomic core. The CI space is formed by a set of configuration with all possible single (S) and double (D) excitations of the valence electrons in a given basis set. We first set the basis set of orbitals as {16s, 16p, 16d, 16f, 16g}, and then increase it up to {26s, 26p, 26d, 26f, 26g} and {29s, 29p, 29d, 29f, 29g}, which leads to the energy change with the expansion of the CI space lower than 0.01% and the matrix elements of the allowed E1 transitions change at most 0.03%. $\hat{h}_2$ is the interaction between the valence electrons. In the CI+MBPT procedure, a single-electron operator which represents the correlation interaction of a particular valence electron with the atomic core is added into $\hat{h}_1$. A two-electron operator which represents the screening of the Coulomb interaction between the two valence electrons by the core electrons is added into $\hat{h}_2$. Both additional operators are treated in the second order of MBPT.

2.3. MCDHF calculations

To verify the hybrid CI+MBPT calculations, the MCDHF method is used in this work, as it is another form of CI method and based on the variational principle with both expansion coefficients and the orbitals to be variational parameters so that take into account correlations in a different way. The MCDHF calculations in this work are performed using the GRASP2018 package.[24]

In the MCDHF method, the calculation starts with the many-electron Dirac–Coulomb Hamiltonian

$$\hat{H}_{\text{DC}} = \sum_i^N \left(c\boldsymbol{\alpha}_i \cdot \boldsymbol{p}_i + (\beta_i - 1)c^2 + V_i\right) + \sum_{j>i}^N \frac{1}{r_{ij}}, \tag{6}$$

where $\boldsymbol{\alpha}_i$ and β_i are usual 4×4 Dirac matrices, and $\boldsymbol{p}_i$ is the one-electron momentum operator, c is the speed of light, V_i is the electron–nucleus Coulomb attraction for a finite nucleus. The nuclear charge distribution is modeled by the two-component Fermi function.[26] An atomic state wavefunction (ASF) Ψ is constructed as a linear combination of configuration state functions (CSFs) Φ of the same parity P, the total angular momentum J and its projection M_J, which is written as

$$\Psi(\gamma PJM_J) = \sum_{i=1}^{N_{\text{CSF}}} c_i \Phi(\gamma_i PJM_J). \tag{7}$$

where c_i is expansion (mixing) coefficient, γ_i stands for the remaining quantum numbers of the CSFs. Each CSF is a linear combination of products of one-electron Dirac orbitals. Both mixing coefficients and orbitals are optimized in the self-consistent field calculation. After a set of orbitals is obtained, the relativistic configuration interaction (RCI) calculations are used to capture more electron correlations. In addition to the Coulomb interactions, our RCI calculations also include the Breit interaction in the low-frequency approximation and the quantum electrodynamic (QED) corrections.

In the present MCDHF calculations, the CSF space of a specified P and J symmetry is generated following the active set (AS) approach[27,28] by virtual excitations from the orbitals in multireference (MR) configurations to an active set of orbitals. By extending the AS systematically, the CSF space is increased and thereby approaches the complete representation of the ASF with Eq. (7). The ASFs of even and odd states are optimized separately and the MR configuration sets for even and odd parities include

$$\begin{aligned} \text{even}: &\ 3s^2,\ 3p^2,\ 3s4s,\ 3s5s,\ 3s3d,\ 3s4d, \\ \text{odd}: &\ 3s3p,\ 3s4p,\ 3s5p,\ 3s4f. \end{aligned}$$

Initial MCDHF calculations in the RSCF procedure are performed to determine simultaneously all the orbitals of the MR sets without any excitations. Subsequently, the CSFs expansions are obtained through single and double excitations from the orbitals in the MR sets of configurations up to an AS of orbitals with $n \leq 13$, $l \leq 4$. The AS is increased with layer by layer in 8 steps from $n = 6$ up to 13, i.e., AS_1–AS_8, so that the basis set convergence in the calculations can be demonstrated. In each step, only the orbitals in newly added layer are optimized and the other orbitals are kept to be fixed. We treat the orbitals with $n \leq 2$ as the core, and the other orbitals as the valence orbitals. We have allowed single and double excitations from the valence orbitals and single excitations from the core so that both the valence–valence (VV) and core–valence (CV) correlations have been taken into account in the RSCF procedure. In our test calculations, it was found that the contributions from 1s and 2s excitations are not important to the atomic parameters concerned, so these orbitals are kept to be fixed as an inactive core in the final calculational model. The differences between the energy levels obtained with the last two basis set, AS_7 and AS_8, do not exceed 15 cm^{-1} for any level.

Here we also include higher-order correlation effects with a further extended CSF space enlarged by allowing triple (T) excitations from the orbitals in the MR sets to an AS_i ($i \leq 5$) of orbitals obtained in the previous RSCF procedure. It is convenient to define the CSF space in each step of SD-excitations as sdAS_i ($i \leq 8$) and in each step of SDT-excitations as sdAS_8+triAS_i ($i \leq 5$). The differences between the energy

levels obtained with sdAS$_8$+triAS$_4$ and sdAS$_8$+triAS$_5$ do not exceed 10 cm^{-1} for any level. Therefore, the ASFs for every atomic states concerned are finally expanded with the CSF space sdAS$_8$+triAS$_5$ by Eq. (7).

Once the ASFs are obtained, the multipole-radiative transition matrix element from an initial state $\Psi(\gamma PJM)$ to a final state $\Psi(\gamma' P' J' M')$, $\langle \Psi(\gamma PJM) \| \hat{O}^{(k)} \| \Psi(\gamma' P' J' M') \rangle$ can be obtained.

3. Results and discussion

3.1. Energy levels and E1 matrix elements

In the present work, the energy levels and the E1 transition matrix elements of Al^+ are calculated using CI+MBPT method and MCDHF method. The computational details of each method are described in Section 2. The results of the excitation energies from the ground $3s^2\ ^1S_0$ state to the low-lying states of Al^+ obtained using CI+MBPT method with the basis set {29s, 29p, 29d, 29f, 29g}, and using MCDHF method with sdAS$_8$+triAS$_5$ are tabulated in Table 1. It includes 16 odd-parity states with 3s3p, 3s4p, 3s4f and 3s5p configurations, and 17 even-parity states with $3p^2$, 3s4s, 3s3d, 3s5s, and 3s4d configurations. The final results of both CI+MBPT and MCDHF methods show good agreement with the values listed in National Institute of Standards and Technology (NIST) database.[29] It is noted that the discrepancies between the results of CI+MBPT method and NIST data are below 124 cm^{-1} and the relative deviation to NIST data is lower than 0.13%. The energies of CI+MBPT method using pure CI, CI+MBPT without and with Breit interaction procedures are presented. It shows that the combination of CI and MBPT improves the accuracy notably. Although the double excitations from core orbitals are neglected in our MCDHF calculations, the discrepancies between the calculated excitation energies and NIST data are below 400 cm^{-1} and the relative deviation to NIST data is lower than 0.4%. This shows the importance of the VV and CV correlations in the MCDHF calculations on the transition properties of Al^+. The contributions of the triple excitation, Breit interaction, self-energy and vacuum polarization to the final MCDHF results are also listed in the table.

Table 1. The excitation energies (in cm^{-1}) of the low-lying levels of Al^+, obtained by using the CI+MBPT and MCDHF methods and compared with the available values listed in NIST database.[29] T, B., SE and VP denote the triple excitation, Breit interaction, self-energy and vacuum polarization, respectively. $\Delta_1 \equiv E_{\mathrm{CI+MBPT+B.}} - E_{\mathrm{NIST}}$ and $\Delta_2 \equiv E_{\mathrm{MCDHF}} - E_{\mathrm{NIST}}$.

State	NIST	CI+MBPT method				MCDHF method					
		CI	CI+MBPT	CI+MBPT+B.	Δ_1	MCDHF	Contri. T	Contri. B.	Contri. SE	Contri. VP	Δ_2
3s3p $^3P^o_0$	37393.03	36256	37342	37344	–49	37441	–3.30	9.83	–14.33	0.71	48
3s3p $^3P^o_1$	37453.91	36318	37407	37405	–49	37501	6.88	5.00	–14.25	0.72	47
3s3p $^3P^o_2$	37577.79	36443	37539	37530	–48	37623	1.01	–3.34	–14.11	0.72	46
3s3p $^1P^o_1$	59852.02	59538	59905	59893	41	60064	–113.30	–3.56	–14.96	0.69	212
$3p^2\ ^1D_2$	85481.35	83515	85404	85384	–97	85745	22.25	–5.68	–23.15	1.17	264
3s4s $^3S_1$	91274.50	90008	91254	91233	–41	91529	20.33	–7.65	–12.17	0.42	254
$3p^2\ ^3P_0$	94084.96	92597	94041	94034	–51	94228	13.17	5.86	–30.63	1.58	143
$3p^2\ ^3P_1$	94147.46	92660	94107	94097	–50	94289	20.77	1.91	–30.53	1.58	142
$3p^2\ ^3P_2$	94268.68	92782	94236	94219	–49	94409	29.10	–6.65	–30.33	1.57	141
3s4s $^1S_0$	95350.60	94007	95289	95268	–83	95597	–24.91	–7.84	–12.39	0.45	246
3s3d $^3D_3$	95549.42	94169	95490	95461	–89	95944	3.05	–12.68	–14.77	0.65	395
3s3d $^3D_2$	95550.51	94170	95490	95462	–89	95945	19.82	–12.25	–14.79	0.64	395
3s3d $^3D_1$	95551.44	94171	95491	95462	–89	95946	17.57	–11.72	–14.79	0.64	395
3s4p $^3P^o_0$	105427.52	103961	105372	105352	–75	105688	18.64	–4.97	–14.17	0.57	261
3s4p $^3P^o_1$	105441.50	103975	105387	105366	–75	105702	23.25	–6.05	–14.11	0.58	261
3s4p $^3P^o_2$	105470.93	104005	105418	105396	–75	105731	20.79	–8.01	–14.02	0.57	260
3s4p $^1P^o_1$	106920.56	105574	106880	106858	–62	107197	–48.07	–7.14	–13.00	0.63	276
3s3d $^1D_2$	110089.83	108816	110122	110099	9	110425	–56.15	–8.33	–19.77	0.88	335
$3p^2\ ^1S_0$	111637.33	110488	111779	111761	124	112014	–134.56	–5.59	–29.01	1.48	376
3s5s $^3S_1$	120092.919	118590	120047	120022	–70	120394	28.97	–9.29	–13.18	0.50	301
3s5s $^1S_0$	121366.725	119827	121305	121281	–86	121664	19.49	–9.25	–13.64	0.53	297
3s4d $^3D_3$	121483.50	119970	121420	121392	–91	121833	19.11	–11.23	–14.63	0.58	350
3s4d $^3D_2$	121483.92	119971	121421	121394	–90	121833	26.49	–11.04	–14.63	0.59	349
3s4d $^3D_1$	121484.252	119971	121422	121395	–89	121834	25.93	–10.85	–14.64	0.59	349
3s4f $^3F^o_2$	123418.48	121693	123358	123331	–88	123759	–17.84	–9.48	–14.77	0.59	340
3s4f $^3F^o_3$	123420.45	121696	123361	123333	–87	123761	–23.94	–9.71	–14.77	0.58	341
3s4f $^3F^o_4$	123423.36	121699	123364	123336	–87	123764	–23.15	–9.96	–14.74	0.59	341
3s4f $^1F^o_3$	123470.5	121775	123413	123385	–85	123810	–11.25	–9.80	–14.59	0.58	339
3s4d $^1D_2$	124794.13	123377	124784	124757	–37	125190	–60.72	–10.72	–16.09	0.67	396
3s5p $^3P^o_0$	125703.14	124136	125641	125617	–86	126004	27.68	–7.66	–14.20	0.56	301
3s5p $^3P^o_1$	125708.828	124142	125648	125624	–85	126010	31.40	–8.08	–14.17	0.56	301
3s5p $^3P^o_2$	125721.703	124155	125662	125637	–84	126023	29.55	–8.95	–14.14	0.56	301
3s5p $^1P^o_1$	125869.015	124322	125814	125790	–79	126175	–19.07	–8.55	–12.84	0.59	306

Table 2. The reduced matrix elements of E1 transition for the $3s^2\ ^1S_0$ and $3s3p\ ^3P^o_0$ clock states of Al^+, obtained by using the CI+MBPT and MCDHF methods.

Method Guage	CI+MBPT		MCDHF		Recommend	Reference
	Length	Velocity	Length	Velocity		
$3s^2\ ^1S_0 - 3s3p\ ^3P^o_1$	0.0098	0.0105	0.0058	0.0159	0.010(6)	
$3s^2\ ^1S_0 - 3s3p\ ^1P^o_1$	3.1156	3.1688	3.1188	3.1323	3.115(54)	3.112[18]
$3s^2\ ^1S_0 - 3s4p\ ^3P^o_1$	0.0022	0.0018	2.5×10^{-5}	0.0031	0.002(3)	
$3s^2\ ^1S_0 - 3s4p\ ^1P^o_1$	0.0460	0.0737	0.0419	0.0547	0.046(28)	0.045[18]
$3s^2\ ^1S_0 - 3s5p\ ^3P^o_1$	0.0051	0.0043	0.0032	0.0053	0.005(3)	
$3s^2\ ^1S_0 - 3s5p\ ^1P^o_1$	0.0662	0.0491	0.0674	0.0609	0.066(17)	
$3s^2\ ^1S_0 - 3s6p\ ^1P^o_1$	0.0704	0.0586			0.070(12)	
$3s^2\ ^1S_0 - 3s6p\ ^3P^o_1$	0.0023	0.0017			0.002(1)	
$3s^2\ ^1S_0 - 3s7p\ ^1P^o_1$	0.0638	0.0551			0.064(9)	
$3s^2\ ^1S_0 - 3s7p\ ^3P^o_1$	0.0022	0.0019			0.002(1)	
$3s^2\ ^1S_0 - 3s8p\ ^1P^o_1$	0.0505	0.0448			0.051(6)	
$3s^2\ ^1S_0 - 3s8p\ ^3P^o_1$	0.0250	0.0220			0.025(3)	
$3s^2\ ^1S_0 - 3s9p\ ^1P^o_1$	0.0784	0.0718			0.078(7)	
$3s3p\ ^3P^o_0 - 3s4s\ ^3S_1$	0.8979	0.8926	0.8959	0.9015	0.898(8)	0.900[18]
$3s3p\ ^3P^o_0 - 3p^2\ ^3P_1$	1.8394	1.8789	1.8318	1.8590	1.840(39)	1.836[18]
$3s3p\ ^3P^o_0 - 3s3d\ ^3D_1$	2.2350	2.2626	2.2267	2.2252	2.235(28)	2.236[18]
$3s3p\ ^3P^o_0 - 3s5s\ ^3S_1$	0.2690	0.2661	0.2687	0.2706	0.269(3)	
$3s3p\ ^3P^o_0 - 3s4d\ ^3D_1$	0.4456	0.4612	0.4495	0.4498	0.446(16)	
$3s3p\ ^3P^o_0 - 3s6s\ ^3S_1$	0.1505	0.1486			0.151(2)	
$3s3p\ ^3P^o_0 - 3s5d\ ^3D_1$	0.1921	0.2029			0.192(11)	
$3s3p\ ^3P^o_0 - 3s7s\ ^3S_1$	0.0414	0.0422			0.041(1)	
$3s3p\ ^3P^o_0 - 3s6d\ ^3D_1$	0.1097	0.1178			0.110(8)	
$3s3p\ ^3P^o_0 - 3s8s\ ^3S_1$	0.1027	0.1005			0.103(2)	
$3s3p\ ^3P^o_0 - 3s7d\ ^3D_1$	0.0722	0.0787			0.072(6)	
$3s3p\ ^3P^o_0 - 3s9s\ ^3S_1$	0.0991	0.0986			0.099(1)	
$3s3p\ ^3P^o_0 - 3s8d\ ^3D_1$	0.0571	0.0630			0.057(6)	

The E1 RMEs involving the $3s^2\ ^1S_0$ and $3s3p\ ^3P^o_0$ clock states of Al^+ obtained using CI+MBPT and MCDHF methods are presented in Table 2. The results in both length and velocity gauge are listed. The CI+MBPT results in the length gauge agree well with the counterparts obtained using CI+all-order method.[18] The E1 RMEs involving $3s3p\ ^3P^o_0$ state of CI+MBPT and MCDHF method in the same gauge have good agreement with each other, and the relative differences are below 2%. The agreement of the E1 RMEs involving $3s^2\ ^1S_0$ state of both methods in the same gauge is not as good as the E1 RMEs involving $3s3p\ ^3P^o_0$ state and the relative differences span from 0.1% to over 50%. However, we would like to emphasize here that large discrepancies only occur for those RMEs involving weak transitions, which contribute fractionally to the polarizabilities discussed in this work. The discrepancy in the length and velocity gauge of E1 RMEs can be noted for the same theoretical method. Although it can be shown that the length and velocity form of the electric multipole transition operators yield the same line strength for an exact solution in the non-relativistic theory, it is not exactly same in the relativistic Dirac theory.[30,31] It is pointed out that the discrepancies in the length and velocity gauge of the calculated line strengths ($S^O_{v\kappa} = |\langle v\|\hat{O}\|\kappa\rangle|^2$) for E1 transition is an important uncertainty indicator.[31,32] Thus, we also give the recommended values of E1 RMEs in Table 2, and the uncertainties are given following the above suggestion.

3.2. Polorizabilities

The static and dynamic E1 polarizabilities are calculated using Eqs. (1) and (2). The transition energies used in Eq. (2) are cited from NIST data. For the choice of the static polarizability of Al^{3+} core, $\alpha_{\rm core}$, Mitroy *et al.* adopted the value of 0.268 a.u. which is the scaled result obtained from a perturbed HF calculations[16] and Safronova *et al.* adopted 0.265 a.u. in their evaluation the BBR shift of the clock transition in Al^+ using CI+all-order method.[18] We apply the coupled-cluster method with single and double excitations (CCSD) which is implemented in Gaussian09 package[33] associated with a large basis set (aug-cc-pv6z basis set) and get 0.260 a.u. for the Al close-shell core. This result should capture sufficient correlation contribution, but the relativistic effect is absent. In the present work, $\alpha_{\rm core} = 0.265(5)$ a.u. is adopted. Core-valence contributions to the polarizability is usually small, and they are cited from Ref. [18] with a "safe" uncertainty of 50%. The dynamic corrections to $\alpha_{\rm core}$ and $\alpha_{\rm cv}$ follow the extrapolation method used by Brewer *et al.*[9] Static E1 polarizabilities for $3s^2\ ^1S_0$ and $3s3p^3P^o_0$ states are listed in Table 3. The SOS method is adopted for the polarizability calculations in this work. Our calculated values for the static polarizabilities agree with the results from other theoretical work. The uncertainties for the calculated static polarizabilities come from the uncertainties of the E1 RMEs, core and core-valence contribu-

tions. The present differential polarizability also agrees with the experimental result,[9] which is derived from the ac Stark shift measurement using an extrapolation method.

Table 3. The static E1 polarizabilities (in a.u.) of $3s^2\ ^1S_0$ and $3s3p\ ^3P^o_0$ states in Al^+, and the differential polarizabilities.

Method	α_0 ($3s^2\ ^1S_0$)	α_0 ($3s3p\ ^3P^o_0$)	$\Delta\alpha_0$
Present	24.11(82)	24.58(50)	0.47(1.32)
CICP[16]	24.1396	24.6223	0.4827
RCC[17]	24.14(8)	24.61(12)	0.48(8)
CI+all-order[18]	24.048	24.543	0.495(48)
MRCI/MRCC[19]	24.065(410)	24.552(742)	0.487(1.152)
Expt.[9]			0.426(57)

The dynamic polarizabilities $\alpha(\omega)$ of the $3s^2\ ^1S_0$ and $3s3p\ ^3P^o_0$ states in Al^+ are shown in Fig. 1. The photon energies of the electromagnetic radiation from 0 to 0.43 a.u. are taken into account, which is equivalent to the wavelength varying from ∞ down to 106 nm. Five magic wavelengths of the Al^+ $3s^2\ ^1S_0$–$3s3p\ ^3P^o_0$ clock transition are identified, as 267.01(10) nm, 183.18(2) nm, 173.68(2) nm, 120.50(2) nm, and 113.33(48) nm. All magic wavelengths are located in the ultraviolet region. In the our numerical procedures, the magic wavelength is obtained when the dynamic differential polarizability $\Delta\alpha(\omega)$ of $3s^2\ ^1S_0$ and $3s3p\ ^3P^o_0$ states is zero. It can be noted that the core polarizability is same for both clock states and it will not affect the position of the magic wavelength. The uncertainty of the magic wavelength is evaluated by taking account of the uncertainties of the E1 RMEs in the magic wavelength identification procedure.

The contributions of individual transitions to the static and dynamical polarizabilities of the $3s^2\ ^1S_0$ and $3s3p\ ^3P^o_0$ states at the magic wavelengths for the $3s^2\ ^1S_0$–$3s3p\ ^3P^o_0$ clock transition in Al^+ are tabulated in Table 4. It is noted that the contribution of $3s^2\ ^1S_0$–$3s3p\ ^1P^o_1$ transition solely dominates the static and the five dynamic polarizabilities of $3s^2\ ^1S_0$ state at the magic wavelengths, and it contributes no less than 92%. For the static and dynamic polarizabilities of $3s3p\ ^3P^o_0$ state at three magic wavelengths (267.01 nm, 183.18 nm and 173.68 nm), the contributions of three transitions, $3s3p\ ^3P^o_0$–$3s4s\ ^3S_1$, $3s3p\ ^3P^o_0$–$3p^2\ ^3P_1$, and $3s3p\ ^3P^o_0$–$3s3d\ ^3D_1$, are over 95%. Tang *et al.* suggested that the ratio of two oscillator strengths could be determined via the precision measurement of magic wavelength for Ca^+,[34] and it was practiced successfully.[22] By taking similar procedure in Ref. [22] and taking into account the RME of the strongest E1 transition $3s^2\ ^1S_0$–$3s3p\ ^1P^o_1$, the measurement on the magic wavelengths of Al^+ clock transition at 267.01 nm, 183.18 nm, and 173.68 nm would be helpful to obtain three ratios of the E1 RMEs for the four transitions mentioned above, RME($3s^2\ ^1S_0$–$3s3p\ ^1P^o_1$):RME($3s3p\ ^3P^o_0$–$3s4s\ ^3S_1$), RME($3s^2\ ^1S_0$–$3s3p\ ^1P^o_1$):RME($3s3p\ ^3P^o_0$–$3p^2\ ^3P_1$), and RME($3s^2\ ^1S_0$–$3s3p\ ^1P^o_1$):RME($3s3p\ ^3P^o_0$–$3s3d\ ^3D_1$). It can act as a calibration with the experimental input to the calculated RMEs, and then improve the reliability and the precision of the estimate of the BBR shift for the clock transition.

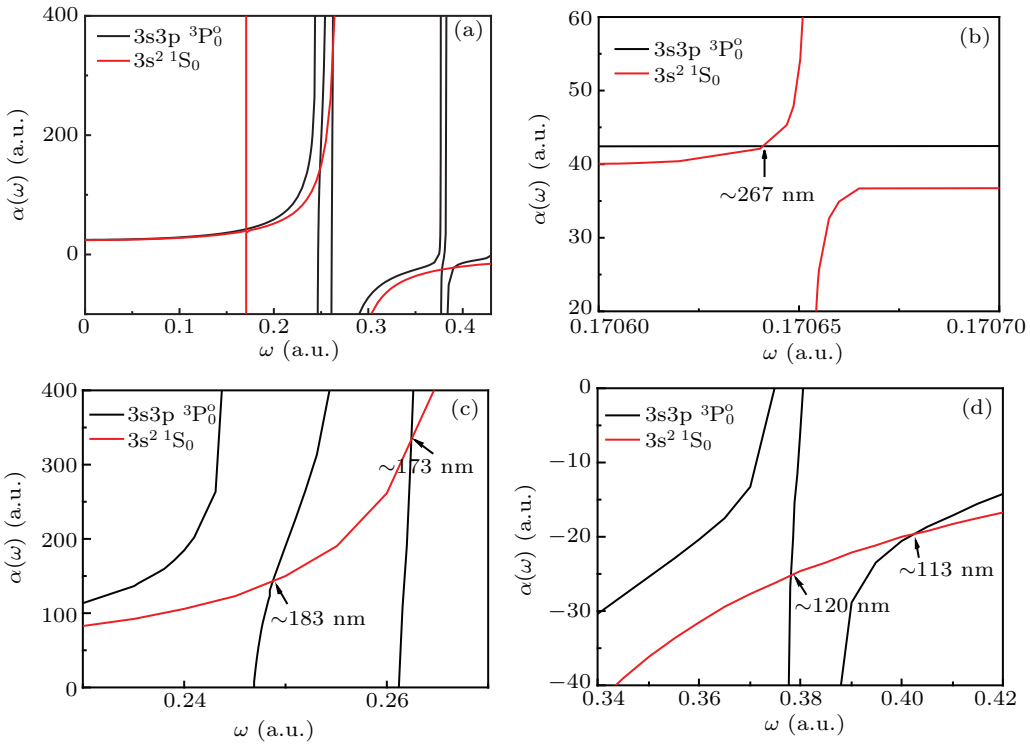


Fig. 1. The dynamic polarizabilities $\alpha(\omega)$ of the $3s^2\ ^1S_0$ and $3s3p\ ^3P^o_0$ states in Al^+, in a photon energy of the electromagnetic radiation from 0.0 to 0.43 a.u., which is equivalent to the wavelength from ∞ down to 106 nm. The magic wavelengths are identified by arrows in (b)–(d).

Table 4. The breakdown of the contributions of individual transitions to the static and dynamical polarizabilities of the $3s^2\,{}^1S_0$ and $3s3p\,{}^3P_0^o$ states at the magic wavelengths for the $3s^2\,{}^1S_0$–$3s3p\,{}^3P_0^o$ clock transition in Al^+. The numbers in parentheses are uncertainties in the digits calculated by adopting the recommended uncertainties of E1 RMEs in the present work.

λ_m (nm)	∞	267.01(10)	183.18(2)	173.68(2)	120.50(1)	113.33(48)
ω_m (a.u.)	0	0.170642(65)	0.248739(33)	0.262338(29)	0.378115(44)	0.402028(1709)
			$\alpha(\omega)$ $(3s^2\,{}^1S_0)$			
$3s^2\,{}^1S_0 - 3s3p\,{}^3P_1^o$	0.0004	3.0500	–0.0003	–0.0003	–0.0001	-0.0001
$3s^2\,{}^1S_0 - 3s3p\,{}^1P_1^o$	23.7209	38.9854	141.1584	318.0193	–25.7146	–20.2169
$3s^2\,{}^1S_0 - 3s4p\,{}^3P_1^o$	6.0×10^{-6}	6.0×10^{-6}	8.0×10^{-6}	8.0×10^{-6}	1.5×10^{-5}	1.9×10^{-5}
$3s^2\,{}^1S_0 - 3s4p\,{}^1P_1^o$	0.0029	0.0033	0.0039	0.0041	0.0073	0.0091
$3s^2\,{}^1S_0 - 3s5p\,{}^3P_1^o$	2.9×10^{-5}	3.2×10^{-5}	3.6×10^{-5}	3.7E-05	0.0001	0.0001
$3s^2\,{}^1S_0 - 3s5p\,{}^1P_1^o$	0.0051	0.0056	0.0062	0.0064	0.0090	0.0100
Others	0.1325	0.1421	0.1547	0.1576	0.1980	0.2116
Core	0.2650	0.2651	0.2657	0.2658	0.2671	0.2671
VC	–0.0190	–0.0191	–0.0191	–0.0192	–0.0193	–0.0194
Total	24.1078	42.4323	141.5690	318.4332	–25.2544	–19.7402
			$\alpha(\omega)$ $(3s3p\,{}^3P_0^o)$			
$3s3p\,{}^3P_0^o - 3s4s\,{}^3S_1$	2.1898	4.2366	–82.4867	–15.4363	–1.5959	–1.3022
$3s3p\,{}^3P_0^o - 3p^2\,{}^3P_1$	8.7283	15.4606	116.7639	–299.0884	–7.6696	–6.1596
$3s3p\,{}^3P_0^o - 3s3d\,{}^3D_1$	12.5671	21.4705	105.7086	631.2767	–12.1297	–9.6541
$3s3p\,{}^3P_0^o - 3s5s\,{}^3S_1$	0.1280	0.1611	0.2269	0.2485	–18.4314	–0.9254
$3s3p\,{}^3P_0^o - 3s4d\,{}^3D_1$	0.3461	0.4317	0.5982	0.6516	13.2613	–3.4274
Others	0.3619	0.4167	0.5029	0.5261	1.0559	1.4735
Core	0.2650	0.2651	0.2657	0.2658	0.2671	0.2671
VC	–0.0100	-0.0100	–0.0101	–0.0101	–0.0102	–0.0102
Total	24.5762	42.4323	141.5690	318.4332	–25.2544	–19.7402

Table 5. The differential dynamic polarizabilities (in a.u.) of the clock states in Al^+.

Wavelength (nm)	1126	976	267.4	397	866
$\alpha(\omega)[3s^2\,{}^1S_0]$	24.64(84)	24.82(85)	39.44(1.41)	29.22(1.00)	25.03(85)
$\alpha(\omega)[3s3p\,{}^3P_0^o]$	25.16(51)	25.37(52)	42.34(86)	30.30(62)	25.59(52)
$\Delta\alpha(\omega)$ (a.u.)	0.52(1.35)	0.54(1.37)	2.90(2.27)	1.08(1.62)	0.56(1.37)

The calculated dynamic polarizabilities can be used to evaluate the ac Stark shifts due to the clock interrogation, cooling, and repumping laser beams of the Al^+ optical clock. Based on the knowledge of the dynamic prolarizabilities obtained in this work, the calculated differential polarizabilities of the Al^+ clock transition at several specific wavelengths are given in Table 5. Rosenband *et al.* measured the ac Stack shift of the Al^+ clock transition using an infrared light at 1126 nm[20] and obtained $\Delta\alpha(\omega) = 1.08(34)$ a.u. CI+all-order method gives this value as 0.549(55) a.u. and CICP method gives as 0.54(41) a.u. Our result agrees with theirs. Brewer *et al.* obtained $\Delta\alpha(976\,\text{nm}) = 0.499(57)$ a.u. in their experiment and our result also agree with it. The wavelength of the clock interrogation beam is 267.4 nm. The cooling (397 nm) and repumping beams (866 nm) are kept on in same experiments to maintain a stable cooling.[35] According to the data in Table 5 and assuming all the laser beams to be Gaussian beams, the contributions of ac Stark shift to the fractional frequencey shift ($\Delta\nu_{\text{ac-Stark}}/\nu_{\text{clock}}$) of Al^+ clock transition at 267.4, 397 and 866 nm are $(1.54\pm1.21)\times10^{-20}\tilde{I}$, $(5.74\pm8.61)\times10^{-20}\tilde{I}$, and $(2.98\pm7.28)\times10^{-21}\tilde{I}$, respectively, where the effective intensity $\tilde{I} = P/r^2$, P is the power of the laser in units of W and r is the radius of beam waist in units of m.

4. Conclusions

In summary, the dynamic polarizabilities of $3s^2\,{}^1S_0$ and $3s3p\,{}^3P_0^o$ states in Al^+ are calculated using CI+MBPT and MCDHF methods in this work. The magic wavelengths for the Al^+ clock transition $3s^2\,{}^1S_0$–$3s3p\,{}^3P_0^o$ are identified. All the magic wavelengths predicted in this work are in the ultraviolet region. The potential precision measurement on these magic wavelengths of Al^+ near 267 nm, 183 nm and 173 nm would be useful to extract the ratios of several certain transition matrix elements with high accuracy, and then to improve the precision of the estimate of the BBR shift for the Al^+ clock transition. The differential dynamic polarizabilities at certain wavelengths are evaluated using the knowledge of the calculated dynamic polarizabilities, which are useful to assess the ac Stark shift of the Al^+ clock transition frequency and helpful in the clock experiments to suppress the ac Stark shift of the clock transition as possible as it can.

Acknowledgements

The authors would like to thank Professor M. G. Kozlov and Dr. Y. M. Yu for the helpful assistance on the use of CI-MBPT package. This work was supported by the National Natural Science Foundation of China (Grant Nos. 11934014, 11904387, 11704076, and U1732140), the National Key Research and Development Program of China (Grant Nos. 2017YFA0304401 and 2017YFA0304402), and Technical Innovation Program of Hubei Province, China (Grant No. 2018AAA045).

References

[1] Derevianko A and Katori H 2011 *Rev. Mod. Phys.* **83** 331
[2] Ludlow A D, Boyd M M, Ye J, Peik E and Schmidt P O 2015 *Rev. Mod. Phys.* **87** 637
[3] Safronova M S, Budker D, DeMille D, Jackson-Kimball D F, Derevianko A and Clark C W 2018 *Rev. Mod. Phys.* **90** 025008
[4] Kozlov M G, Safronova M S, Crespo López-Urrutia J R and Schmidt P O 2018 *Rev. Mod. Phys.* **90** 045005
[5] Huntemann H, Sanner C, Lipphardt B, Tamm C and Peik E 2016 *Phys. Rev. Lett.* **116** 063001
[6] Huang Y, Guan H, Liu P, Bian W, Ma L, Liang K, Li T and Gao K 2016 *Phys. Rev. Lett.* **116** 013001
[7] McGrew W F, Zhang X, Fasano R J, Schäffer S A, Beloy K, Nicolodi D, Brown R C, Hinkley N, Milani G, Schioppo M, Yoon T H and Ludlow A D 2018 *Nature* **564** 87
[8] Oelker E, Hutson R B, Kennedy C J, Sonderhouse L, Bothwell T, Goban A, Kedar D, Sanner C, Robinson J M, Marti G E, Matei D G, Legero T, Giunta M, Holzwarth R, Riehle F, Sterr U and Ye J 2019 *Nat. Photon.* **13** 714
[9] Brewer S M, Chen J S, Hankin A M, Clements E R, Chou C W, Wineland D J, Hume D B and Leibrandt D R 2019 *Phys. Rev. Lett.* **123** 033201
[10] Schmidt P O, Rosenband T, Langer C, Itano W M, Bergquist J C and Wineland D J 2005 *Science* **309** 749
[11] Chou C W, Hume D B, Koelemeij J C, Wineland D J and Rosenband T 2010 *Phys. Rev. Lett.* **104** 070802
[12] Mitroy J, Safronova M S and Clark C W 2010 *J. Phys. B: At. Mol. Opt. Phys.* **43** 202001
[13] Porsev S G and Derevianko A 2006 *Phys. Rev. A* **74** 020502
[14] Shang J J, Cui K F, Cao J, Wang S M, Chao S J, Shu H L and Huang X R 2016 *Chin. Phys. Lett.* **33** 103701
[15] Dalgarno A 1962 *Adv. Phys.* **11** 281
[16] Mitroy J, Zhang J Y, Bromley M W J and Rollin K G 2009 *Eur. Phys. J. D* **53** 15
[17] Kallay M, Nataraj H S, Sahoo B K, Das B P and Visscher L 2011 *Phys. Rev. A* **83** 030503
[18] Safronova M S, Kozlov M G and Clark C W 2011 *Phys. Rev. Lett.* **107** 143006
[19] Yu Y M, Suo B B and Fan H 2013 *Phys. Rev. A* **88** 052518
[20] Rosenband T, Itano W M, Schmidt P O, Hume D B, Koelemeij J C J, Bergquist J C and Wineland D J 2006 *Proceedings of the* 20*th European Frequency and Time Forum*, March 27–30, 2006, Braunschweig, Germany, p. 289
[21] Katori H, Takamoto M, Palćhikov V G and Ovsiannikov V G 2003 *Phys. Rev. Lett.* **91** 173005
[22] Liu P L, Huang Y, Bian W, Shao H, Guan H, Tang Y B, Li C B, Mitroy J and Gao K L 2015 *Phys. Rev. Lett.* **114** 223001
[23] Kozlov M G, Porsev S G, Safronova M S and Tupitsyn I I 2015 *Comput. Phys. Commun.* **195** 199
[24] Fischer C F, Gaigalas G, Jönsson P and Bieroń J 2019 *Comput. Phys. Commun.* **237** 184
[25] Manakov N L, Ovsiannikov V D and Rapoport L P 1986 *Phys. Rep.* **141** 320
[26] Parpia F A, Fischer C F and Grant I P 1996 *Comput. Phys. Commun.* **94** 249
[27] Olsen J, Roos B O, Jrgensen P and Jensen H J A 1988 *J. Chem. Phys.* **89** 2185
[28] Sturesson L, Jönsson P and Fischer C F 2007 *Comput. Phys. Commun.* **177** 539
[29] Kramida A, Ralchenko Yu, Reader J and NIST ASD Team 2020 *NIST Atomic Spectra Database* (ver. 5.8), [Online]. Available: https://physics.nist.gov/asd. National Institute of Standards and Technology, Gaithersburg, MD.
[30] Grant I P 1974 *J. Phys. B: At. Mol. Opt. Phys.* **7** 1458
[31] Fischer C F 2009 *Phys. Scr. T* **2009** 014019
[32] Ekman J, Godefroid M R and Hartman H 2014 *Atoms* **2** 215
[33] Frisch M J, Trucks G W, Schlegel H B, *et al.* 2016 *Gaussian 09*, Revision B 01, (Gaussian, Inc., Wallingford CT)
[34] Tang Y B, Qiao H X, Shi T Y and Mitroy J 2013 *Phys. Rev. A* **87** 042517
[35] Chao S J, Cui K F, Wang S M, Cao J, Shu H L and Huang X R 2019 *Chin. Phys. Lett.* **36** 120601